10.1109/ULTSYM.2009.0360

An Efficient Formulation for Harmonic Waves in Multilayered Cylindrical Structures

Ergun Simsek
Bahcesehir University
Besiktas, Istanbul, TURKEY 34349

Bikash K. Sinha
Schlumberger-Doll Research
1 Hampshire Street, Cambridge, MA 02139-1578

Abstract— Equations of motion for harmonic waves in multilayered cylindrical structures are given in a compact form. This compact form helps us to efficiently form a boundary condition matrix of any N-layer structure based on material parameters for all cylindrical layers. Fluid-fluid, fluid-solid, and solid-fluid boundaries are supported. The search algorithm automatically searches for zeros of a boundary-condition determinant that yields the borehole velocity dispersion for a given frequency band. We describe how to obtain radial displacements and stress amplitudes for a chosen frequency that can be useful in estimating frequency dependent radial depth of investigation for the borehole Stoneley, flexural, and quadrupole modes in the presence of a casing and tool effects on sonic data. An efficient formulation for calculating borehole dispersions plays an important role in the analysis and interpretation of measured borehole dispersions in the presence of a sonic tool structure and radially heterogeneous formation. Applications of this formulation in the analysis of field data will be presented.

Keywords: Elastic wave propagation; multilayered cylindrical structures; borehole waves

I. INTRODUCTION

Sonic techniques in geophysical prospecting involve elastic wave velocity measurements that are performed by placing acoustic transmitters and receivers in a fluid-filled borehole [1-7]. However, generally the geometry is more complicated than this. For example, a heavy fluid model can be used to account for the effect of a logging tool which makes it a 3-layer structure. A steel collar is used to meet the strength requirements for tough logging conditions encountered in deviated and horizontal drilling. In addition steel casing is cemented to a formation that also introduces additional cylindrical layers in the logging environment. Moreover, Sinha *et al.* [8] have shown that the effect of near-wellbore alteration can be simulated by using several layers back to back where the layer parameters change gradually from casing properties to formation parameters. In this case, number of layers can be as large 20.

Even though different configurations create different boundary conditions to be satisfied, from the sonic data analysis point of view, the ultimate goal is the same, i.e., process the signals recorded at an array of receivers to obtain compressional and shear wave velocities in the surrounding formation. These velocities are generally used in seismic surveys for the time-to-depth conversion and for estimating other formation parameters, such as porosity and lithology. Depending upon the type of transmitter used and as a result of eccentering, one can excite axisymmetric (n=0), flexural (n=1), and quadrupole (n=2) family of modes propagating along the borehole.

Sinha *et al.* have studied an open hole (2-layer) and a steel pipe in a fluid-filled borehole configuration in detail in [9, 10] and described how to build boundary condition matrices to obtain modal amplitudes for 2 and 4-layer cases. The aim of this work is to extend this approach to any *N*-layer structure.

To this end, we first present a very general way of writing equations of motion for harmonic waves in multilayered cylindrical structures. Next, we describe an efficient method to form a boundary condition matrix whose determinant vanishes for certain frequency-slowness values that defines the slowness dispersion of a guided mode. The size of the matrix depends on the number of cylindrical layers and the type of boundary conditions. From the computational point of view, the number of layers can go up to 36 for $n \geq 1$, and up to 50 for $n = 0$, if double precision is used, which allows us to invert matrices as big as 200×200 accurately.

II. MATHEMATICAL FORMULATION

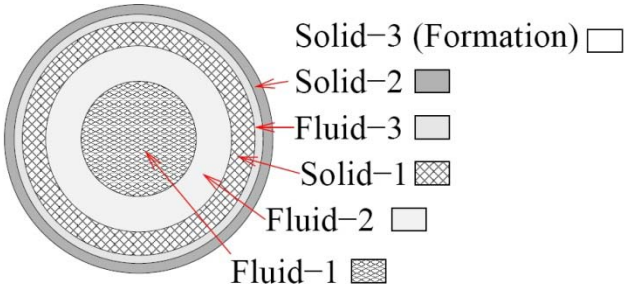

Figure 1 Six-layer geometry: fluid-1 (from center to r = e), fluid-2 (from r = e to r = d), solid-1 (from r = d to r = c), fluid-3 (from r = c to r = b), solid-2 (from r = b to r = a), and solid-3 (formation, from r = a to r = ∞).

Equations of motion for harmonic waves in cylindrical structures are given in [11]. A set of solutions for an open hole and a concentric steel pipe in a water-filled borehole are given in [9, 10, 12]. Here, we present a more general way of writing these equations which makes it possible to analyze any kind of multilayered cylindrical structures.

Assume that we have an *N*-layer cylindrical structure, where each layer is an isotropic material. Layer-*m* is defined by ρ_m, $V_{c,m}$ and $V_{s,m}$ which are mass density, compressional and shear wave velocities, respectively. Figure 1 shows an example of 6-layer geometry where the inner-most layer (a cylindrical

column) is the heavy-fluid column (tool); between the tool and casing, we have borehole fluid, between the casing and formation, we first have a thin liquid, then a solid layer. In this configuration, we have fluid-fluid, fluid-solid, and solid-solid boundaries.

In earlier papers [9, 10, 12], equations of motions for harmonic waves are written with the variables of τ_{rr}, $\tau_{\theta\theta}$, τ_{zz}, τ_{rz}, $\tau_{r\theta}$, and $\tau_{z\theta}$ which are the stress components; u_r, u_θ, and u_z which are the displacement components. One can establish a search routine to find the resonant mode velocities (V) for a given frequency (f) in a (f, V) search domain. Here we have a slightly different search domain (Ω, ζ), where $\Omega = \omega a/V_{s,N}$ and $\zeta = ka$ which is converted to (f, V) by using

$$V = \Omega V_{s,N}/\zeta, \qquad f = \Omega V_{s,N}/2\pi a, \qquad (1)$$

where $\omega=2\pi f$ is the radial frequency, $a = r_{N-1}$ is the borehole radius, k is the resonant mode's wavenumber. Figure 2 shows an example of the conversion from one domain to another one for a flexural mode discussed in the Numerical Results section. The blue circles denote zeros of boundary condition determinant matrix in (Ω, ζ) space. Red, green, and cyan dashed lines show formation compressional and shear velocities, and fluid compressional, respectively. (b) Slowness-frequency dispersion (f, V) obtained from results in Figure 2a.

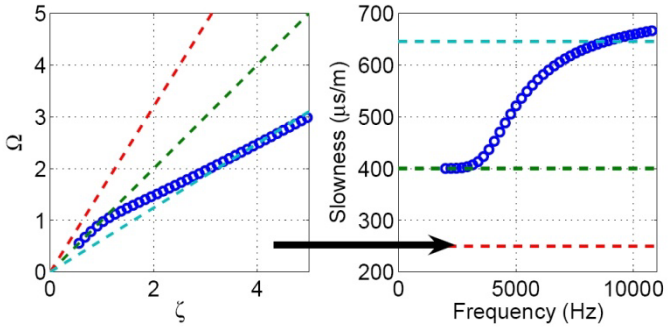

Figure 2 (a) The blue circles denote zeros of boundary condition determinant matrix in (Ω, ζ) space. Red, green, and cyan dashed lines show formation compressional and shear velocities, and fluid compressional, respectively. (b) Slowness-frequency dispersion (f, V) obtained from results in Figure 2a.

In this work we look for the zeros of determinant matrix for a fixed ζ value over a range of Ω values. To speed up this process, which has to be done for each ζ separately, we can narrow the range by putting upper and narrow limits. For example, we know that resonant mode has to occur for a velocity (V) value, which is slower than or equal to the formation shear velocity. It should also be noted that Ω can be complex; in this case mode search domain becomes a two-dimensional domain and the transformation in Eq. 1 should be carried out by using the real part of Ω.

Expressing the displacement components in cylindrical coordinates in terms of a standard scalar and vector potentials and using constitutive relations for a homogeneous material, we obtain general expressions for the displacement and stress components as follows

$$u_\Lambda(r,\Omega,\zeta) = \sum_{p=1}^{6} C_p^{(m)} \tilde{u}_\Lambda^{(m)}(r,\Omega,\zeta), \qquad (2)$$

$$\tau_\Xi(r,\Omega,\zeta) = \sum_{p=1}^{6} C_p^{(m)} \tilde{\tau}_\Xi^{(m)}(r,\Omega,\zeta), \qquad (3)$$

where Λ is r, θ, or z; Ξ is rr, $r\theta$, or rz; $C_p^{(m)}$'s are unknown coefficients to be determined in the m^{th} layer. The elements of Eq.s 2 and 3 are given in Tables I, II, III, and IV. The detail of the formulation is as follows. For the inner-most layer ($m=0$), $F_n^\psi = J_n(\psi_m r)$ and $G_n^\psi = 0$, while ψ_m is either α_m or β_m; for the outer-most layer ($m = N$), $F_n^\psi = H_n(\psi_m r)$ and $G_n^\psi = 0$; for other layers ($1<m<N$), $F_n^\psi = J_n(\psi_m r)$ and $G_n^\psi = Y_n(\psi_m r)$. Here, J_n and Y_n are n^{th} order first and second kind Bessel functions and H_n is n^{th} order Hankel function of second kind.

$$\alpha_m^2 = (\Omega V_{s,N} V_{c,m})^2 - \zeta^2, \qquad (4)$$

$$\beta_m^2 = \begin{cases} 0, & \text{if } V_{s,m} = 0 \\ (\Omega V_{s,N} V_{s,m})^2 - \zeta^2, & \text{otherwise.} \end{cases} \qquad (5)$$

Table 1Displacement Components

p	$\tilde{u}_r^{(m)}(r,\Omega,\zeta)$	$\tilde{u}_\theta^{(m)}(r,\Omega,\zeta)$	$\tilde{u}_z^{(m)}(r,\Omega,\zeta)$
1	$\frac{n}{r}F_n^\alpha - \alpha_m F_{n+1}^\alpha$	$-\frac{n}{r}F_n^\alpha$	$i\zeta F_n^\alpha$
2	$\frac{n}{r}G_n^\alpha - \alpha_m G_{n+1}^\alpha$	$-\frac{n}{r}G_n^\alpha$	$i\zeta G_n^\alpha$
3	$i\zeta F_{n+1}^\beta$	$i\zeta F_{n+1}^\beta$	$-\beta_m F_n^\beta$
4	$i\zeta G_{n+1}^\beta$	$i\zeta G_{n+1}^\beta$	$-\beta_m G_n^\beta$
5	$\frac{n}{r}F_n^\beta$	$-\frac{n}{r}F_n^\beta + \beta_m F_{n+1}^\beta$	–
6	$\frac{n}{r}G_n^\beta$	$-\frac{n}{r}G_n^\beta + \beta_m G_{n+1}^\beta$	–

Table 2 Stress Component: $\tilde{\tau}_{rr}^{(m)}(r,\Omega,\zeta)/\mu_{(m)}$

p	$\tilde{\tau}_{rr}^{(m)}(r,\Omega,\zeta)/\mu_{(m)}$
1	$-(\lambda_{(m)}/\mu_{(m)}(\alpha_m^2+\zeta^2)$ $+2(\alpha_m^2 - n(n-1)/r^2))F_n^\alpha + 2\alpha_m F_{n+1}^\alpha/r$
2	$-(\lambda_{(m)}/\mu_{(m)}(\alpha_m^2+\zeta^2)$ $+2(\alpha_m^2 - n(n-1)/r^2))G_n^\alpha + 2\alpha_m G_{n+1}^\alpha/r$
3	$2i\zeta(\beta_m F_n^\beta - (n+1)F_{n+1}^\beta/r)$
4	$2i\zeta(\beta_m G_n^\beta - (n+1)G_{n+1}^\beta/r)$
5	$2n((n-1)F_n^\beta/r^2 - \beta_m F_{n+1}^\beta/r)$
6	$2n((n-1)G_n^\beta/r^2 - \beta_m G_{n+1}^\beta/r)$

Table 3 Stress Component: $\tilde{\tau}_{r\theta}^{(m)}(r,\Omega,\zeta)/\mu_{(m)}$

p	$\tilde{\tau}_{r\theta}^{(m)}(r,\Omega,\zeta)/\mu_{(m)}$
1	$2n((1-n)F_n^{\alpha}/r^2+\alpha_m F_{n+1}^{\alpha}/r)$
2	$2n((1-n)G_n^{\alpha}/r^2+\alpha_m G_{n+1}^{\alpha}/r)$
3	$i\zeta(\beta_m F_n^{\beta}-2(n+1)F_{n+1}^{\beta}/r)$
4	$i\zeta(\beta_m G_n^{\beta}-2(n+1)G_{n+1}^{\beta}/r)$
5	$(\beta_m^2+2n(1-n)/r^2)F_n^{\beta}-2\beta_m F_{n+1}^{\beta}/r$
6	$(\beta_m^2+2n(1-n)/r^2)G_n^{\beta}-2\beta_m G_{n+1}^{\beta}/r$

Table 4 Stress Component: $\tilde{\tau}_{rz}^{(m)}(r,\Omega,\zeta)/\mu_{(m)}$

p	$\tilde{\tau}_{rz}^{(m)}(r,\Omega,\zeta)/\mu_{(m)}$
1	$2i\zeta(nF_n^{\alpha}/r-\alpha_m F_{n+1}^{\alpha})$
2	$2i\zeta(nG_n^{\alpha}/r-\alpha_m G_{n+1}^{\alpha})$
3	$-n\beta_m F_n^{\beta}/r+(\beta_m^2-\zeta^2)F_{n+1}^{\beta}$
4	$-n\beta_m G_n^{\beta}/r+(\beta_m^2-\zeta^2)G_{n+1}^{\beta}$
5	$i\zeta n F_n^{\beta}/r$
6	$i\zeta n G_n^{\beta}/r$

Note that we use only first four terms when $n = 0$, for the lowest order axi-symmetric mode.

The unknown amplitudes associated with different cylindrical layers are determined by satisfying the appropriate boundary conditions at the relevant interfaces. The solution to a cylindrically layered system can be obtained by satisfying appropriate boundary conditions at all the interfaces. These conditions can be expressed in terms of a matrix equation $\boldsymbol{L}c = 0$, where the vector c denotes the unknown amplitude coefficients. For nontrivial solutions of this matrix equation, we require that the determinant of coefficient matrix $\boldsymbol{L}$ be zero. By the provided formulation, we can form the $\boldsymbol{L}$ matrix automatically by inserting appropriate stress and velocity elements into corresponding boundary conditions at various interfaces. When we obtain $|\boldsymbol{L}| = 0$ for a given pair of Ω *and* ζ, we know the mode velocity for a given frequency. We can then obtain the amplitude ratios by assigning one of the $C_p^{(m)}$ to an arbitrary number and calculate the other $C_p^{(m)}$ values.

Table 5 Material Properties of a 6-Layer Geometry

m	ρ (g/cm^3)	$V_{c,m}$ (m/s)	$V_{s,m}$ (m/s)	r_{inner} (cm)
1	5000	1000	-	0
2	1000	1550	-	5
3	7900	5800	3100	8
4	1050	1500	-	9
5	2850	4050	2550	10
6	2800	4000	2500	11

II. Computational Results

Consider a 6-layer geometry, as shown in Figure 1. The material properties of each layer are given in Table V. To check the accuracy of our formulation and implementation, we first obtain borehole slowness dispersions by using the Green's function formulation [13]. This formulation yields synthetic waveforms at an array of receivers produced by a monopole, dipole or quadrupole source placed on the borehole axis. Synthetic waveforms are then processed by a modified matrix pencil algorithm [14] to isolate both non-dispersive and dispersive arrivals in the wavetrain. For this problem, we use 21 receivers. The distance between the source and first receiver is 1 m and inter-receiver spacing is 10 cm.

Figure 3 shows the borehole slowness dispersions for a monopole ($n = 0$), a dipole ($n = 1$), and a quadrupole ($n = 2$) modes obtained by processing the recorded synthetic waveforms by a modified matrix pencil algorithm (blue crossed lines) and the Mode Search algorithm (red circles) described in this work. The results reveal a very good agreement between these two different formulations.

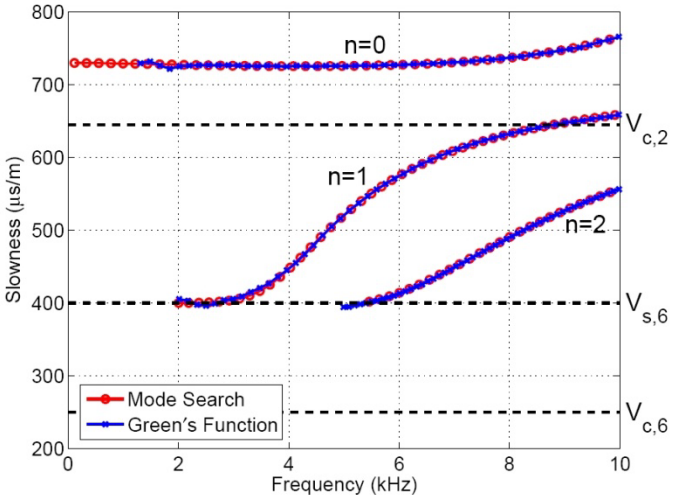

Figure 3 Comparison of slownesses obtained with a Mode Search algorithm (red circles) and Green's Function approach (blue crosses) for n = {0, 1, 2}.

Next we plot relative displacement and stress amplitudes for the three different modes shown in Figure 3 at f = 6 kHz in Figures 4, 5, and 6. u_r and τ_{rr} components show continuity for all of the cases, as expected. However, for the other components we observe jumps on the interfaces. The shear stress τ_{rz} is always zero in inviscid liquids.

III. Conclusions

We present an efficient way of writing equations of motion for harmonic waves in multilayered cylindrical structures. This compact form enables us to obtain boundary condition matrix and radial displacement and stress amplitudes in a systematic way. The accuracy of the algorithm is validated by comparing results from the Green's function method. This work would help in the analysis and interpretation of sonic response in open as well as cased holes in the presence of near-wellbore alteration and tool effects.

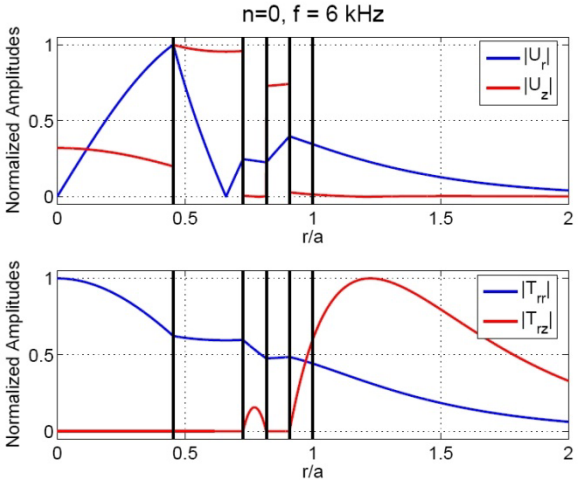

Figure 4 Radial variations of (a) displacements, and (b) stress amplitudes associated with the Stoneley mode at 6 kHz. Black vertical lines depict interfaces between different layers.

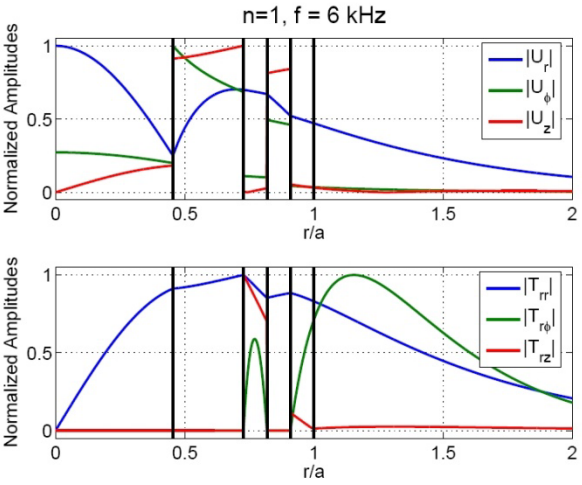

Figure 5 Follows the notation in Figure 5 for a dipole source.

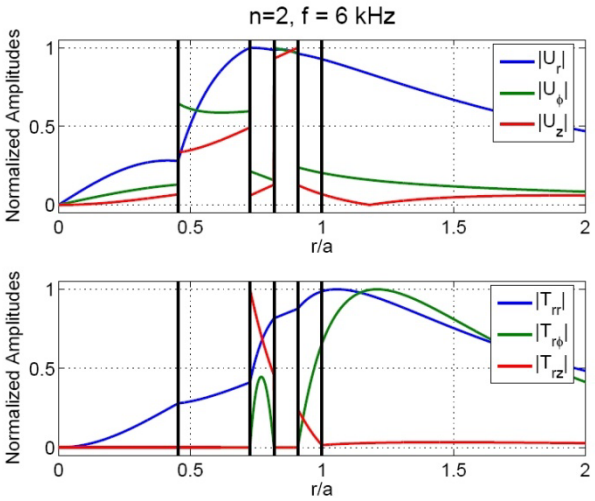

Figure 6 Follows the notation in Figure 4 for a quadrupole source.

REFERENCES

[1] Kurkjian, A. L., 1985, Numerical computation of individual far-field arrivals excited by an acoustic source in a borehole: Geophysics, 50, 852–866.

[2] Kurkjian, A. L., and Chang, S. K., 1986. Acoustic multipole sources in fluid-filled boreholes. Geophysics, 51, pp. 148-163.

[3] Stevens, J.L. and Day, S.M., 1986. Shear velocity logging in slow formations using the Stoneley wave. Geophysics, 51, pp. 137–147.

[4] Paillet F. L. and Cheng, C.H., 1991. Acoustic Waves in Boreholes, Chapter 8, CRC Press, Boca Raton, FL.

[5] Zemanek, J., Williams, D.M., and Schmitt, D.P., 1991. Shear-wave logging using multipole sources. The Log Analyst, 32, No. 3, pp. 233–241.

[6] Schmitt, D.P., 1988. Shear Wave Logging in Elastic Formations. J. Acoust. Soc. A., 84(6), pp. 2215–2229.

[7] Kimball, C.V., 1998. Shear slowness measurement by dispersive processing of the borehole flexural mode. Geophysics, 63, pp. 337–344.

[8] Sinha, B.K., Vissapragada, B., Renlie, L. & Tysse, S., 2006. Radial profiling of the three formation shear moduli and its application to well completions. Geophysics, 71(6), E65–E77.

[9] Sinha, B.K. and Asvadurov, S., 2004. Dispersion and radial depth of investigation of borehole modes. Geophysical Prospecting, 52(4), pp. 271–286.

[10] Sinha, B.K., Simsek, E. & Asvadurov, S., 2008. Influence of a pipe tool on borehole modes. To be published in Geophysics, May-June 2009.

[11] Gazis, D., 1959. Three-dimensional investigation of the propagation of waves in hollow circular cylinders, I. Analytical foundation, and II. Numerical Results. J. Acoust. Soc. Am., 31, pp. 568–577.

[12] Hsu, C. J. and Sinha, B. K., 1998. Mandrel effects on the dipole flexural mode in a borehole. J. Acoust. Soc. Am., 104(4), pp. 2025–2039.

[13] Lu, C.C. and Liu, Q.H., 1994. Three-dimensional dyadic Green's function for elastic waves in multilayer cylindrical structures. J. Acoust. Soc. Am., 96(5), pp. 3337–3338.

[14] Ekstrom, M., 1995. Dispersion estimation from borehole acoustic arrays using a modified matrix pencil algorithm. 29th Asilomar Conference on Signals, Systems and Computers, Pacific Grove, CA.